# Evaluation of Subject Contrast and Normalized Average Glandular Dose by Semi-Analytical Models

A. Tomal[1], M.E. Poletti[1], L.V. Caldas[2]

[1] Departamento de Física e Matemática, Faculdade de Filosofia, Ciências e Letras de Ribeirão Preto, Universidade de São Paulo, Ribeirão Preto, SP, Brazil.
poletti@ffclrp.usp.br

[2] Instituto de Pesquisas Energéticas e Nucleares, Comissão Nacional de Energia Nuclear, São Paulo, SP, Brazil

## Abstract

In this work, two semi-analytical models are described to evaluate the subject contrast of nodules and the normalized average glandular dose in mammography. Both models were used to study the influence of some parameters, such as breast characteristics (thickness and composition) and incident spectra (kVp and target-filter combination) on the subject contrast of a nodule and on the normalized average glandular dose. From the subject contrast results, detection limits of nodules were also determined. Our results were in good agreement with those reported by others authors, who had used Monte Carlo simulation, showing the robustness of our semi-analytical method.

**Keywords:** Mammography; subject contrast; detection limits; normalized average glandular dose

## 1 – Introduction

Mammography is, nowadays, the most effective and accurate method for early detection of breast cancer. Since mammography is always associated with a small risk of carcinogenesis, it is important to establish an optimization criterion between image quality and breast dose (Dance, 1990; Wu *et al.*, 1991; Dance *et al.*, 2000a). The first step to achieve this optimization is to evaluate the image quality and the absorbed dose in mammography for different examination parameters.

The image quality is usually evaluated in terms of contrast, noise and unsharpness (Carlsson *et al.*, 1986; Vyborny and Schmidt, 1994). In screen-film mammography the image contrast is the main quality index, and it is dependent on subject contrast and on film contrast, which are independent of each other (Wagner, 1991). Several works have investigated the factors that affect the subject contrast (*SC*) of microcalcifications within a breast (Wagner, 1991; Dance and Day, 1992; Gingold *et al.*, 1995; Dance *et al.*, 2000b; Delis *et al.*, 2006). However, less extensive data are available for subject contrast of nodules (Wagner, 1991). The subject contrast determination has been performed in most of the previous works by Monte Carlo simulation (Dance and Day, 1992; Dance *et al.*, 2000b; Delis *et al.*, 2006), although Carlsson *et al* (1986) proposed an analytical model, which could be applied to compute *SC* values in a mammographic examination. A similar semi-analytical model was employed by Leclair and Johns (2002) to compute the contrast only due to scattered radiation.

The average absorbed dose by glandular tissue is the most appropriate information for risk assessments associated with mammography (Dance, 1990; Dance *et al*, 2000a). However, direct measurement of this quantity is difficult, and in most practical situation it is derived from the product of the measured entrance air Kerma and appropriate conversion factors of normalized average glandular dose (Dance, 1990; Wu *et al.*, 1991, 1994; Dance *et al*, 2000a). These conversion factors can be computed using basically two approaches: from measured depth dose data (Hammerstein, 1979) or using Monte Carlo simulation (Dance, 1990; Wu *et al.*, 1991, 1994; Dance *et al*, 2000a). Among these methods, the determination by Monte Carlo simulation is the most used, since it eliminates some limitations in the measurements (e.g. variation of the dose laterally, breast phantom composition and geometry).

In summary, these quantities (subject contrast and normalized average glandular dose) are usually determined by experimental and simulation (Monte Carlo) methods, which are time demanding. Thus the development of analytical models to study these parameters in a fast and simple way would be outstanding.

In this work, we describe semi-analytic models, which were developed to determine the subject contrast and the normalized average glandular dose in mammography. The model for the subject contrast computation takes both primary and scatter (single and double) contributions into account in the transmitted x-ray intensity. The model for the normalized average glandular dose includes the contribution of single and double interactions in the computation of the fraction of energy absorbed by the glandular tissue. Both semi-analytical models were used to study the influence of some parameters, such as breast characteristics (thickness and composition) and incident spectra (kVp and target-filter combination), on the subject contrast of a nodule and on the normalized average glandular dose. From the subject contrast results, detection limits of nodules were also determined.

## 2 – Materials and Methods

### *2.1 – Geometrical model*

The compressed breast was represented by a half cylinder, with area of 100 $cm^2$ and variable thicknesses between 2 and 8 cm. The tissue distribution inside the object was considered as an homogeneous mixture of adipose and glandular tissue uniformly distributed in the central region and enclosed by a 0.5 cm adipose layer both upper and lower surface. The glandular content of the breast tissue was varied from 0% to 100% in order to represent several breast compositions. The detection system was considered as composed by a $Gd_2O_2S$:Tb phosphor screen of mass thickness 33.4 $mg/cm^2$ (compatible with Kodak Min-R 2000) and a Kodak Min-R 2000 film. A 65 cm source-to-image receptor distance was considered. The x-ray beam was perpendicular to the entrance surface, and uniformly distributed. In this preliminary work the grid was not considered.

Specifically to study the subject contrast, a small contrasting detail (with cubic form) was included within the breast at an arbitrary distance from the surface. This detail (nodule) was considered as

composed by malignant breast tissue with thickness varying between 0.1 and 1 cm. The detail area was considered large enough to neglect unsharpness effect.

### *2.2 – Sources of the models: x-ray spectra, compositions data and cross-section*

The mammographic spectra utilized in this study were computed using a spectral model developed by Boone *et al.* (1997). The X-ray spectra were calculated for Mo and Rh anode materials, operating at tube voltages from 24 kVp to 35 kVp, and filtered with appropriated k-edge filters (Mo and Rh). The spectra were also modified by the addition of a sheet of 2 mm polycarbonate plastic (compression paddle). These spectra were normalized to produce the same air kerma of 8.764 mGy. The half value layer (HVL) in *mm* Al and the mean energy were determined for each spectrum using the model proposed by Kharrati and Zarrad (2003).

The elemental compositions and density of the breast tissues were taken from Hammerstein *et a1*. (1979). The linear attenuation coefficients of normal and malignant breast tissues were obtained from Tomal *et al.* (2008), while those for the phosphor screen were obtained from the X-COM Database[1]. Differential cross-sections for the incoherent and coherent scattering were computed using the independent atomic model. The corresponding atomic form factor ($F$) and incoherent atomic function ($S$) were obtained from Hubbell *et al.* (1975).

### *2.3 - Subject Contrast*

The subject contrast (*SC*) was calculated using the following relation, introduced by Carlsson *et al.* (1986) and Wagner (1991)

$$SC = \ln\left(\frac{q_B}{q_D}\right) \tag{1}$$

where $q_B$ and $q_D$ are the energies imparted to the receptor per unit area beside and behind the contrasting detail, respectively. Considering that these quantities can be separated in the primary (*p*) and scatter (*s*) components, and assuming that $q_{Bs} = q_{Ds} = q_s$, Eq. 1 becomes:

$$SC = \ln\left(1 + \frac{\left(q_{B_P} - q_{D_P}\right)}{q_{B_P}\left(q_{D_P}/q_{B_P} + q_s/q_{B_P}\right)}\right) \tag{2}$$

In this work the primary contributions $q_{B_P}$ and $q_{D_P}$ were calculated using the Eq. (3) and (4), previously proposed by Carlsson *et al*. (1986).

$$q_{B_P} = \int_E E \times \phi_E(E) \times IF(E) \times e^{-\mu_B . L} dE \tag{3}$$

[1] Available at http://physics.nist.gov/xcom.

$$q_{D_P} = \int_E E \times \phi_E(E) \times IF(E) \times e^{-\mu_B . L} e^{-(\mu_D - \mu_B).x} dE \quad (4)$$

where $E$ is the photon energy, $\phi_E(E)$ is the photon fluence, *IF(E)* is the x-ray detection efficiency, $\mu_B$ and $\mu_D$ are, respectively, the linear attenuation coefficient of the breast and the contrasting detail, $L$ and $x$ are the thicknesses of the breast and the detail, respectively. The x-ray detection efficiency was estimated as the maximum value, assuming that all photon that interact with the system deposited in single interaction its energy (i.e. no secondary photons escape), as suggested by Motz and Danos (1978).

The scatter component ($q_s$) was computed taken into account only the contributions of single and double scattered photon by the breast on the detection system. The single scatter contribution was calculated according to the simple approach proposed by Magalhães *et al.* (1995), while the double scatter contribution was estimated using the method proposed by Wong *et al.* (1981). This latter contribution can represent from 15 to 40% of the single scatter depending on the breast thickness and composition. The comparison of our $q_S / q_{B_p}$ ($= S/P$) values with those obtained from Dance *et al.* (1992) showed a close agreement (~7%), demonstrating that the first and second order scatter contributions are the major contributions on the scatter radiation transmitted.

### *2.4 - Normalized average glandular dose*

The normalized average glandular dose ($D_{gN}$) was calculated using the Eq. (5),

$$D_{gN} = c \times \frac{1}{w_g \times \rho \times (L - 2a)} \times \left\{ \int E \times \phi_E(E) \times G(E) \times \alpha(E)\ dE \right\} \quad (5)$$

where $c$ is a unit conversion factor, $a$ is the thickness of the shield layer, $\rho$ and $L$ are the breast density and thicknesses, respectively, $(L-2a) \times \rho \times w_g$ represents the ratio between the mass of glandular tissue within the breast and the irradiated area, the factor $G(E)$ is used to convert the absorbed energy in the whole breast to the energy absorbed only in the glandular tissue, and $\alpha(E)$ is the fraction of incident energy absorbed by the breast.

The $G(E)$ factors were calculated using the mass energy absorption coefficients $(\mu_{en}/\rho)$ for adipose and glandular tissues, as proposed by Boone (1999).

The $\alpha(E)$ fraction was computed considering only the contribution of first and second interactions on the absorbed energy. Initially, the incident beam (monoenergetic and parallel) was attenuated by the top adipose layer. The energy absorbed in this layer was not included in the dose computation. Then, the central region of the breast was divided into parallel slices, perpendicular to the cylinder symmetry axis. The number of first interactions in each slice was calculated by $N_k(E) = N_0 . \left(e^{-\mu .\ dz.(k-1)}\right) \times \left(1 - e^{-\mu\ .dz}\right) \times \left(e^{-\mu_s .a}\right)$, where $E$ is the photon energy, $\mu$ and $\mu_s$ are the linear attenuation coefficients of the breast and adipose tissues, respectively, $N_0$ is the number of incident

photons with energy $E$, $dz$ is the slice thickness and the index $k$ represent the $k$th slice. The average energy absorbed in the breast due to the first interactions in each slice was computed using the relation $E_{1,\ abs} = \sum_k E \times N_k(E) \times \mu_{en}/\mu$, where $\mu_{en}$ is the linear energy-absorption coefficient of the breast. The next step was to compute the energy deposited in the breast due to the second interactions. For this, the number of photons scattered at different directions was computed according to their differential scattering cross sections, and the point of interaction was assumed uniformly distributed on the area perpendicular to the incident beam. The number of second interactions was calculated and the respective absorbed energy $E_{2,\ abs}$ was numerically evaluated by a similar way to that used to first interactions. Finally, the fraction of absorbed energy due to the first and second interaction, $\alpha(E)$, was computed by $\alpha(E) = \left(E_{1,abs} + E_{2,abs}\right) \Big/ \sum_j E \times N_0$. It is worth to mention that the contribution of the second interactions on the fraction $\alpha(E)$ represented between 4 and 40% of its value, depending on the breast thickness and photon energy. This large contribution shows the importance to include the second interactions on the $D_{gN}$ values.

## 3 – Results and Discussions

### *3.1 – Subject Contrast*

The influence of the breast thickness and composition on the subject contrast is shown in Fig. 1a for a Mo/Mo target-filter combination at 28 kVp. The subject contrast decreases up to 90% with increasing the breast thickness and glandular content. It can be explained by two facts: the primary contrast decreases due to beam hardening by thicker breasts and the ratio $S/P$ increases for large thicknesses (Dance *et al.*, 1992, 2000b; Gingold *et al.*, 1995).

Fig. 1b shows the dependency of the subject contrast with the incident spectra for an average breast (50% glandular) of thickness 5cm. The subject contrast is greater for Mo/Mo spectra than for Rh/Rh spectra at lower tube potentials. However, increasing the kVp from 28 to 35, the subject contrast decreases up to 35, 21 and 17% for Mo/Mo, Mo/Rh and Rh/Rh spectrum, respectively. This is attributed to the reduction of the contrast with increasing X-ray tube potential. The intersection between the curves, shown in Fig. 1b, is due to the spectrum of the transmitted radiation by the breast, and the intersection point depends on the breast thickness and composition.

Finally, based on the results for subject contrast, detection limits were estimated for nodules composed by malignant breast tissue. For this, we considered a screen-film combination describe above, and assumed a gross optical density of 1.4 associated with the background, which is a typical value for screen-film mammography. Fig. 2 shows the subject contrast as a function of the nodule size embedded in an average breast of thickness 2, 4, 6 and 8 cm, using a Mo/Mo spectrum at 28 kVp. The threshold values

of subject contrast corresponding to differences in optical density between 2 and 6% (these values were determine considering that the human vision can discriminate theses differences in optical density) also were included in Fig 3 in order to illustrate the detection limits. This figure shows detection limits between 1.2 and 3.2 mm for an average breast of 4 cm, depending on the contrast threshold. As breast thickness increases, for 6 and 8 cm, the detection limits increases up to 32 e 68%, respectively. Moreover, the detection limits decrease by a factor of about 2 if the contrasting object is embedded in a pure adipose breast, and increases by a factor about 3 for a pure glandular breast. These results are in agreement to those from Brodie and Gutcheck (1982) (between 2 and 4 mm) and from Del Guerra *et al.* (2002) using a signal-to-noise ratio (SNR) threshold value (between 3 and 5 mm).

### *3.2 – Normalized Average Glandular Dose*

The results for the factors of the normalized average glandular dose as a function of the thickness and composition of the breast are shown in Table 1. The values were calculated for a Mo/Mo spectrum at 28 kVp (HVL=0.35 mm Al). The $D_{gN}$ values decrease with increasing the breast thickness and glandularity by up to 75%. The values of Table 1 were compared with those published by Zoetelief and Jansen (1995) and Dance *et al.* (2000a) showing differences up to 9%. These differences were greater for adipose breast and lesser for glandular breast. These discrepancies can be due to x-ray spectra, interactions cross-sections, and mainly, due to the semi-analytical approach used to obtain $\alpha(E)$ values. Particularly, it was observed that these differences are higher for thicker breasts. This was expected because our model neglects the multiple scattering that becomes more probable with increasing the breast thickness.

The influence of the incident spectra on $D_{gN}-$factors is shown in Table 2 for an average breast (50% glandular) of 5cm. For a given kVp and anode-filter combination, the $D_{gN}$ values increase up to 9% with increasing the HVL, as shown in Table 2. For the complete range studied in this work, a large variation (up to 20%) with the HVL was found. The $D_{gN}$ values also increase with the kVp. Although the variation showed in Table 2 is small, the variation can be up to 10% for a large variation in kVp and constant HVL. From Table 2, it can be seen that the $D_{gN}$ values for a Mo/Mo spectra are smaller than for Mo/Rh and Rh/Rh by approximately 3% and 8%, respectively. In summary, the general behaviors of our data are in agreement with observation of Wu *el al* (1991, 1994) and Dance *et al.* (2000a).

## 4 – Conclusions

In this work we illustrate two semi-analytic models that provide a simple and accurate mean to calculate subject contrast and normalized average glandular dose in mammography. Both semi-analytical models were used to study the influence of some parameters, such as breast characteristics (thickness and composition) and incident spectra (kVp and target-filter combination) on the subject contrast of a nodule and on the normalized average glandular dose. The obtained results were in good agreement with those

reported by others authors, who had used Monte Carlo simulation (Dance, 1990; Wu *et al*, 1991, 1994; Zoetelief and Jansen, 1995; Dance *et al*, 2000a). These facts show that higher orders of interactions can be neglected without creating large errors compared with Monte Carlo simulations, simplifying the analytical models. However, for large breasts, the developed models could be improved, including higher orders of interactions, in order to provide more precise results of subject contrast and normalized average glandular dose. Finally, this study allows predictions of detection limits for nodules for different breast thickness and composition.

**Acknowledgements**

This work was supported by the Brazilian agencies Fundação de Amparo à Pesquisa do Estado de São Paulo (FAPESP) and Coordenação de Aperfeiçoamento de Pessoal de Nível Superior (CAPES).

**References**

Boone, J.M., Fewell, T.R., Jennings, R.J., 1997. Molybdenum, rhodium, and tungsten anode spectral models using interpolation polynomials with application to mammography. Med. Phys. 24, 1863-1875.

Boone, J.M., 1999. Glandular Breast dose for monoenergetic and high-energy X-ray beams: Monte Carlo Assessment. Radiology 213, 23-37.

Brodie, I., Gutcheck, R.A., 1982. Radiographic information theory and application to mammography. Med. Phys. 9, 79-94.

Carlsson, G.A., Carlsson, C.A., Nielsen, B., Persliden, J., 1986. Generalized use of contrast degradation and contrast improvement factors in diagnostic radiology. Application to vanishing contrast. Phys. Med. Biol. 31, 737-749.

Dance, D.R., Day, D.R., 1984. The computation of scatter in mammography by Monte Carlo methods. Phys. Med. Biol. 29, 237-247.

Dance, D.R., 1990. Monte Carlo Calculation of conversion factors for the estimation of mean glandular breast dose. Phys. Med. Biol. 35, 1211-1219.

Dance, D.R., Persliden, J., Carlsson, G.A., 1992. Calculation of the dose and contrast for two mammographic grids. Phys. Med. Biol. 37, 235-248.

Dance, D.R., Skinner, C.L., Young, K.C., Beckett, J.R., Kotre, C.J., 2000a Additional factors for the estimation of mean glandular breast dose using the UK mammography dosimetry protocol. Phys. Med. Biol. 45, 3225-3240.

Dance, D.R., Klang, A.T., Sandborg, M., Smith, A.C., Carlsson, G.A., 2000b. Influence of anode/filter material and tube potential on contrast, signal-to-noise ratio and average absorbed dose in mammography: a Monte Carlo study. Brit. J. Radiol. 73, 1056-1067.

Del Guerra, A., Belcari, N., Bencivelli, W., Motta, A., Righi, S., Vaiano, A., Di Domenico, G., Moretti, E., Sabba, N., Zavattini, G., Campanini, R., Lanconelli, N., Riccardi, A., Cinti, M.N., Pani, R., Pellegrini, R., 2002. Monte Carlo study and experimental measurements of breast tumor detectability with the YAP-PEM prototype. Ieee T. Nucl. Sci. 3, 1887- 1891.

Delis H., Spyrou G., Costaridou L., Tzanakos G., Panayiotakis G., 2006. Suitability of new anode materials in mammography: Dose and subject contrast considerations using Monte Carlo simulation, Med. Phys. 33, 4221-4235.

Gingold, E.L., Wu, X., Barnes, G.T., 1995. Contrast and Dose with Mo-Mo, Mo-Rh and Rh-Rh Target-Filter Combinations in mammography. Radiology 195, 639-644.

Hammerstein, G.R., Miller, D.W., White, D.R., Masterson, M.E., Woodard, H.Q., Laughlin, J.S., 1979. Absorbed radiation dose in mammography. Radiology 130, 485-491.

Hubbel, J.H., Veigele, W.J., Briggs, E.A., Brown, R. T., Cromer, D.T., Howerton, R.J., 1975. Atomic form factors, incoherent scattering functions and photon scattering cross sections. J. Phys. Chem. Ref. Data 4, 471-538.

Kharrati, H., Zarrad, B., 2003. Computation of beam quality parameters for Mo/Mo, Mo/Rh, and W/Al target/filter combinations in mammography. Med. Phys. 30, 2638-2642.

Leclair, R.J., Johns, P.C., 2002. Optimum momentum transfer arguments for x-ray forward scatter imaging. Med. Phys. 29, 2881-2890.

Magalhães, S.D., Eichler, J., Gonçalves, O., 1995. Calculation on X-ray scattering of 17,4 keV radiation and image degradation in mammography. Nucl. Instrum. Meth. B 95, 87-90.

Motz, J.W., Danos, M., 1978. Image information content and patient exposure. Med. Phys. 5, 8-22.

Skubic, S.E., Fatouros, P.P., 1986. Absorbed Breast Dose: Dependence on Radiographic Modality and Technique, and Breast Thickness. Radiology 161, 263-270.

Tomal, A., Mazarro, I., Kakuno, E.M., Poletti, M.E., 2008. Experimental Determination of Linear Attenuation Coefficient of Normal, Benign and Malignant Breast Tissues. Submitted to Radiat. Phys. Chem.

Vyborny, C.J., Schimidt, R.A., 1994. Technical Image Quality and the Visibility of Mammographic Detail. RSNA Categorical Course in Physics 103-111.

Zoetelief J., Jansen J.T.M., 1995. Calculation of Air Kerma to Average Glandular Tissue Dose Conversion Factors for Mammography. Radiat. Prot. Dosim. 57, 397-400.

Wagner, A.J., 1991. Contrast and Grid Performance in Mammography. In: Barnes, G.T., Frey, G.D., eds. Screen film mammography: imaging considerations and medical physics responsibilities. Madison, Wis: Med. Phys, 115-134.

Wong, J.W., Henkelman, R.M., Fenster, A., Johns, H.E. 2nd Scatter Contribution to Dose in a Co-60 Beam. Med. Phys 8, 775-782.

Wu, X., Barnes, G.T., Turker, D.M.,1991. Spectral Dependence of glandular tissue dose in screen-film mammography. Radiology 179, 143-148.

Wu, X., Barnes, G.T., Gingold, E.L., Turker, D.M., 1994. Normalized average glandular dose in Molybdenum Target-Rhodium Filter and Rhodium Target-Rhodium Filter mammography. Radiology 193, 83-89.

**FIGURE CAPTIONS**

**Fig. 1** – (a) Subject contrast as a function of the breast thickness and composition, for a nodule of 2 mm and a Mo/Mo spectrum at 28 kVp. (b) Subject contrast as a function of kVp for a breast 50% adipose-50% glandular of 5 cm of thickness with a nodule of 2 mm in three different spectra (Mo/Mo, Mo/Rh and Rh/Rh).

**Fig. 2 –** Subject contrast versus nodule size at averages breast of 2, 4, 6 and 8 cm. (--) represent the contrast thresholds between 2 and 4%.

## TABLES

**Table 1 –** Normalized average glandular dose as a function of breast thickness and compositions. Mo/Mo spectrum at 28 kVp (HVL = 0.35 *mm*Al).

| Breast Thickness (cm) | Breast Glandularity | | |
|---|---|---|---|
| | 0% | 50% | 100% |
| 2.0 | 0.454 | 0.411 | 0.369 |
| 3.0 | 0.345 | 0.294 | 0.25 |
| 4.0 | 0.272 | 0.223 | 0.183 |
| 5.0 | 0.222 | 0.176 | 0.142 |
| 6.0 | 0.185 | 0.145 | 0.115 |
| 7.0 | 0.157 | 0.122 | 0.097 |
| 8.0 | 0.137 | 0.105 | 0.083 |

**Table 2 –** Influence of the incident spectra on the normalized average breast dose for an average breast of 5 cm.

| kVp | HVL (*mm* Al) | Anode-Filter Combination | | |
|---|---|---|---|---|
| | | Mo/Mo | Mo/Rh | Rh/Rh |
| 26 | 0.36 | 0.182 | 0.188 | -- |
| 28 | 0.36 | 0.186 | 0.192 | 0.200 |
| | 0.38 | 0.194 | 0.200 | 0.208 |
| | 0.40 | 0.202 | 0.209 | 0.218 |
| 30 | 0.40 | 0.204 | 0.210 | 0.221 |
| 32 | 0.42 | 0.214 | 0.220 | 0.234 |

**FIGURES**

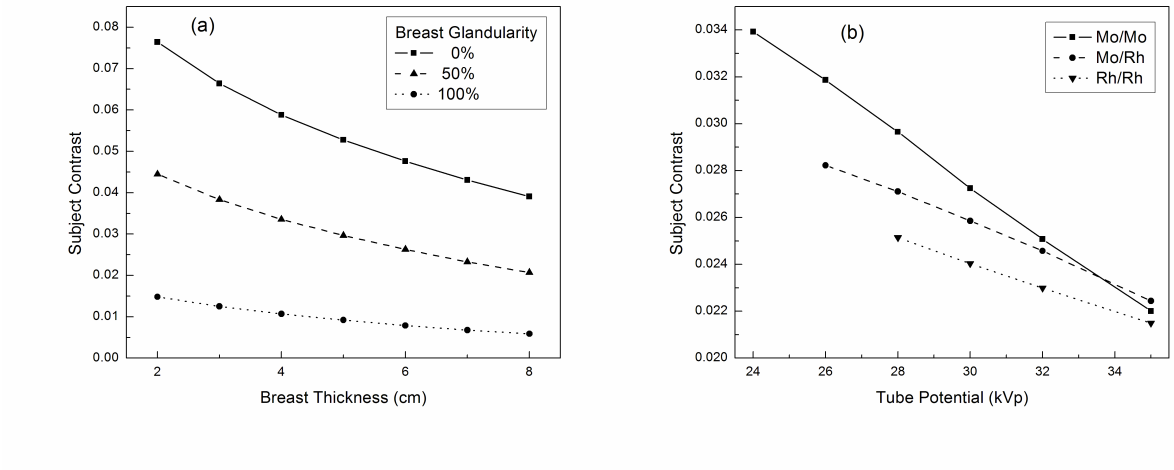


Fig. 1

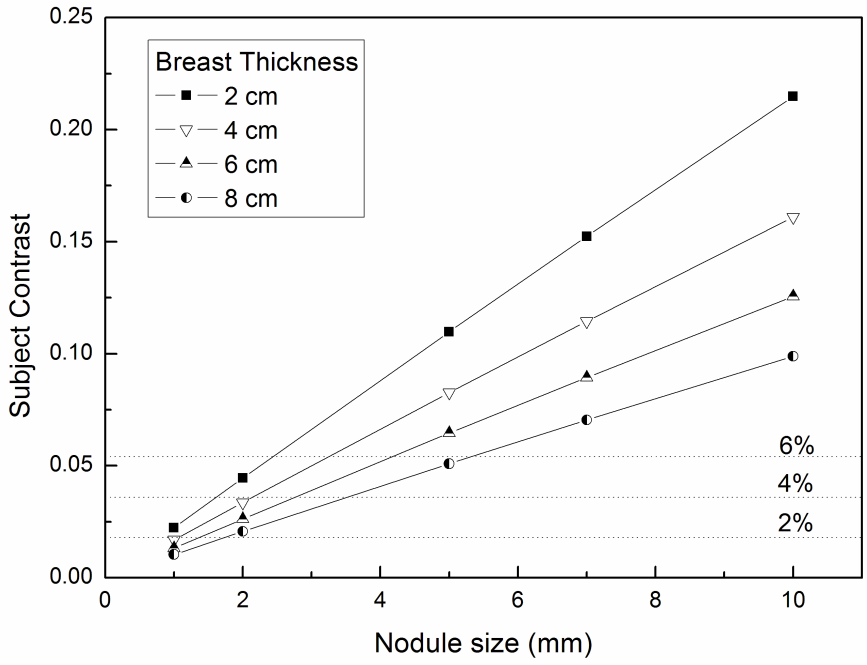


Fig. 2